Reconstruction of potential energy landscapes from local transition probability in microfluidic channels

Yizhou Tan, Alice Thorneywork, Jannes Gladrow, and Ulrich F. Keyser
Cavendish laboratory, University of Cambridge, United Kingdom

Sebastian Sturm
Institut für Theoretische Physik, Universität Leipzig, Germany

Stefano Pagliara*
Living Systems Institute, University of Exeter, Exeter EX4 4QD and
Cavendish laboratory, University of Cambridge, United Kingdom
(Dated: March 10, 2019)

The potential energy landscape of a system, which can be calculated from trajectories of Brownian motion, provides a way to explore the inherent randomness of nature. Using an experimental system of colloidal particles in a microfluidic channel, we show how to extract the underlying potential landscape by analysing local transition probabilities through Bayesian rules. Our method is conceptually similar to the established splitting probability method and, like the splitting probability method, is applicable both to equilibrium systems and nonequilibrium steady states. However, compared to the splitting probability method, our approach offers improved robustness in the face of fragmented trajectories or small trajectory ensembles. We furthermore show how to conveniently implement our approach using probabilistic programming languages, which provides us with systematic error estimates. Our method requires no special experimental instruments and can be easily applied to other trajectory collecting systems.

I. INTRODUCTION

Trajectories of Brownian motion are collected via a range of experimental methods to rebuild the potential energy landscapes of various systems. This acts as a useful tool to understand complicated natural processes. For example, (i) Free energy landscapes have long been used to understand the origin of molecular processes such as protein binding, through force spectroscopy measures [1, 2]. (ii) DNA traces have been recorded by fluorescence microscopy and electrophoresis to explore entropic effects at the nano-scale [3–5]. (iii) Trajectories of colloidal particles are widely used to explore hydrodynamic interactions [6–8], stochastic resonance [9, 10], optical ratcheting and sorting [11–13].

There are two conventional ways to reconstruct a time-stationary free energy landscape, denoted as $U(x)$, from Brownian trajectories. Firstly in an equilibrium system, the probability density function (PDF) of a large enough ensemble of single-particle trajectories relates to a Boltzmann distribution that directly reflects the underlying $U(x)$ [14–16]. However, most situations in living matter are inherently far from equilibrium [17, 18] therefore cannot be analysed using the PDF method. As such, the splitting probability (SP) has recently emerged as an alternative method that removes this limitation. SP is the probability that a particle starting at $x_0 \in [a, b]$ reaches a before it gets b, where $[a, b]$ is the defined analysis interval. Given a large enough ensemble of single-particle trajectories which each end at a or b, SP can be inverted to reliably infer the underlying free energy landscape, as has recently been demonstrated in single-molecule experiments [19, 20].

However, for both PDF and SP, collecting large enough data ensembles from intrinsically stochastic processes remains a challenge. Data collection normally involves lengthy experiments for unstable reactions or rare events. For example, the probability of a particle undergoing Brownian motion across a potential with an energy well scales exponentially with the depth of the well, which could make the experiment unimplementable in practice due to time constancy. Meanwhile experimental data often contains a number of short fragmented trajectories which do not reach the end of the interval. These fragmented trajectories do not readily generate enough long single-particle trajectories required by the SP method so they are excluded from the analysis.

In this paper, a new analysis method, the Local Transition Probability (LTP) is developed to estimate $U(x)$ from fragmented trajectories, both under equilibrium and non-equilibrium conditions. Following the rules of Bayesian statistics, individual LTP is used to estimate the underlying energy landscape through a Gaussian propagator. This method is demonstrated in our colloidal channel experimental system. Compared to the SP method, our LTP method depicts the underlying $U(x)$ more accurately with less noise from the same trajectory ensemble, providing a better estimate of potentials in complex and realistic circumstances as found in experiment.

* s.pagliara@exeter.ac.uk

II. THEORY

In order to compare our new LTP method to existing methods, three methods are used to rebuild potential energy landscapes in this paper:

I. Probability Density Function

The PDF approach [14] assumes that the system is in thermal equilibrium with respect to the underlying $U(x)$, such that

$$p(x) \approx A \exp(-U(x)/k_B T). \tag{1}$$

Here, $p(x)$ denotes the probability to find a particle in a bin centred at x (*i.e.,* one pixel of the camera), k_B is the Boltzmann constant, T is the absolute temperature, and A is a power-dependent normalization constant. For notational convenience, $U_{PDF}(x)$ is defined as the potential landscape reconstructed via Eq. 1.

II. Splitting Probability

As a baseline for non-equilibrium methods, the SP approach earlier introduced by [19] is implemented. Formally, $\pi(x)$ is defined as the probability that a particle starting at $x \in [a, b]$ reaches a before reaching b, as sketched in Fig. 1(a). $\pi(x)$, is measured experimentally by considering the ends of a one-dimensional (1D) channel as a and b.

Given a time-stationary $U(x)$, the splitting probability $\pi(x)$ of an overdamped particle can be derived analytically from the Smoluchowski equation (here assuming a spatially constant diffusion coefficient $D(x) \equiv D$):

$$\pi(x) = \frac{\int_x^b e^{U(x)/k_B T} \mathrm{d}x}{\int_a^b e^{U(x)/k_B T} \mathrm{d}x}. \tag{2}$$

Inverting Eq. 2 allows us to obtain an estimate of the underlying $U(x)$, denoted as $U_{SP}(x)$.

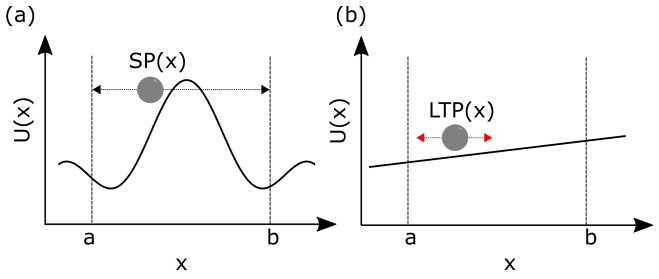

FIG. 1. Sketch of Splitting Probability (SP) and Local Transition Probability (LTP) in typical potential energy landscapes. (a) The SP is defined by the probability of a particle exit through the left absorbing boundary a compared to b. (b) The LTP is defined by the probability of a particle at x to move to the left direction compared to the right.

III. Local Transition Probability

We propose a different method that roughly follows the spirit of the SP method by measuring a particle's transition event to move leftward. If the particle is observed at x' one video frame time after it had been observed at x, we consider that a transition event. Overall we get the LTP along x which is the probability that a particle is moving leftward one video frame later, as illustrated in Fig. 1(b). Compared to the definition of $\pi(x)$, we can get more statistics from LTP by analysing the same trajectory ensemble. Take one particle starting at the centre of the channel for example, we get one count for SP after the particle exits the channel. However, we can collect much more LTP counts during the diffusion of the particle before it gets the channel end.

The LTP of a particle at position x, denoted as $\phi(x)$ can be written down with the PDF of the particle $p(x)$ as

$$\phi(x) = \frac{\int_{-\infty}^{x} p(x)\,\mathrm{d}x}{\int_{-\infty}^{x} p(x)\,\mathrm{d}x + \int_{x}^{\infty} p(x)\,\mathrm{d}x} \tag{3}$$

To find the relationship between $\phi(x)$ and $U(x)$, we first write down the average position displacement of a particle $x_{mean}(x)$ and the mean square displacement (MSD) of a particle in a potential energy landscape:

$$x_{mean}(\delta x, \Delta t) = e^{-\frac{\Delta t \kappa}{\zeta}} \left(\delta \mathrm{x} - \frac{F}{\kappa}\right) + \frac{F}{\kappa} \tag{4}$$

$$MSD(\Delta t) = \frac{k_B T \left(1 - e^{-\frac{2\Delta t \kappa}{\zeta}}\right)}{\kappa} \tag{5}$$

where $F(x) = \frac{\mathrm{d}U(x)}{\mathrm{d}x}$ denotes the force landscape, ζ is the friction coefficient of the particle, κ is the local spring constant of the potential. The detailed deduction can be found in Appendix A.

The probability density $p(x)$ of a diffusion particle starting at x_0 is a Gaussian propagator, where

$$p(x|x_0) = A \frac{\exp\left(\frac{-(x - x_{mean}(x_0, \Delta t))^2}{2MSD}\right)}{\sqrt{2\pi MSD}} \tag{6}$$

Putting Eq. 4 and 5 into Eq. 6, we obtain the relation between p and F

$$p(x|x_0) = A \frac{\exp\left(-\frac{\left(\coth\left(\frac{D\Delta t\kappa}{k_B T}\right) - 1\right)\left((\kappa x - F) e^{\frac{D\Delta t\kappa}{k_B T}} + F - \kappa x_0\right)^2}{4\kappa k_B T}\right)}{\sqrt{2\pi}\sqrt{\frac{k_B T - k_B T e^{-\frac{2D\Delta t\kappa}{k_B T}}}{\kappa}}} \tag{7}$$

where Δt denotes the inverse of the frame rate and D is diffusion coefficient of the particle.

Combining Eq. 3 and 7, we are able to use LTP to estimate $F(x)$ and $U(x)$.

III. EXPERIMENTAL SETUP

We make microfluidic devices as previously reported [21, 22]. Briefly, each device is made of glass and Polydimethylsiloxane, and consists of two 12 μm deep reservoirs connected by an array of channels with a length of 4.8 μm and a cross section of around 0.9×0.9 μm^2. We fill the device with polystyrene colloidal particles with a diameter of (510 ± 10) nm. The particles freely diffuse in the reservoirs but are restricted to single file diffusion within the channels. A typical bright field image of a particle in the channel is shown in Fig. 2(a). We use holographic optical tweezers (HOTs) [16, 23–26] to position the particle and generate optical potential landscapes in each channel. The optical potential landscape is monitored by an infrared camera [Fig. 2(b)] and sketched in Fig. 2(c). Videos of the movement of each particle are recorded by a CCD camera. The trajectories of particles $x(t)$ [Fig. 2(d)] are extracted off-line from the recorded videos using a custom implementation of Crocker and Grier's algorithm [27].

Our drag-and-release measurements consist of six steps as illustrated in Fig. 2(e): I. We trap a single particle diffusing in either reservoir using HOTs. II. We position the particle at a position chosen randomly from an uniform distribution along the channel. III. We use HOTs to set up laser line traps which produce local potential wells. IV - VI. We release the particle and record its trajectory until it escapes from the channel. This process is repeated at least 100 times for each potential landscape configuration.

Using the procedure described above, we are able to obtain single-particle trajectories that can be analyzed with the PDF and SP approaches, which allows us to directly compare with our LTP method under realistic conditions.

IV. TRAJECTORY ANALYSIS

When we apply the LTP method to analyse particle diffusion experiments, the x axis along the microfluidic channel is split into bins. Our notion of what constitutes a transition explicitly does not refer to the particle crossing the boundary from bin i to bin $i-1$, but to what we can measure experimentally: if the particle is observed at some bin $j < i$ one video frame after it had been observed at bin i, that constitutes a transition event. Using this definition, it is irrelevant whether there had been intermediate transitions between i and j, or even to the opposite direction $k > i$. We rewrite Eq. 3 as

$$\phi_i \approx \frac{\int_{-\infty}^{x_i-\Delta x/2} p(x \mid x_i)\,\mathrm{d}x}{\int_{-\infty}^{x_i-\Delta x/2} p(x \mid x_i)\,\mathrm{d}x + \int_{x_i+\Delta x/2}^{\infty} p(x \mid x_i)\,\mathrm{d}x} \quad (8)$$

where $p(x \mid x_i)$ is the PDF of particles starting at x_i diffusing along x, x_i denotes the centre of the i-th bin,

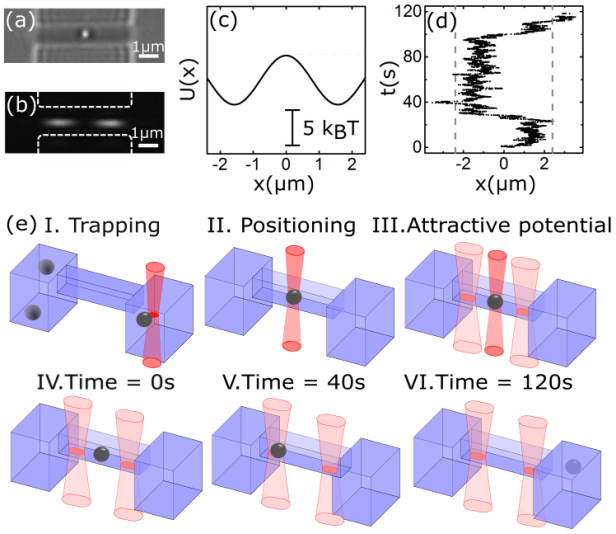

FIG. 2. Experimental approach for measuring potential landscapes in microfluidic channels. (a) Bright-field image of a polystyrene particle trapped in the centre of a microfluidic channel. (b) Dark-field image of the intensity distribution of two laser line traps generated by using HOT. The dashed lines highlight the channel contour. (c) Sketch of the potential wells generated by the two laser line traps in the channel. (d) Sample trajectory of one particle diffusing in the channel. The dashed lines indicate the ends of the channel. (e) Protocol illustration of drag-and-release measurement.

Δx is the bin size, and the approximate relation between ϕ_i and its right-hand side expression becomes exact in the limit $\Delta x \to 0$.

Our approach is readily formulated in a way that can be implemented by modern probabilistic programming tools, given the experimental set of transition counts $|(i \leftarrow)|$, $|(i \rightarrow)|$ where

$$\begin{aligned}(i \leftarrow) \equiv &\{\text{video frame pairs } (n, n+1)\\ &\text{where } x(n) = i \text{ and } x(n+1) < i\},\\ (i \rightarrow) \equiv &\{\text{video frame pairs } (n, n+1)\\ &\text{where } x(n) = i \text{ and } x(n+1) > i\},\end{aligned}$$

the transition counts should follow a binomial distribution with position-dependent parameters,

$$\begin{aligned}\mathbb{P}(|(i \leftarrow)| = k \in [0, \ldots, n_i]) &= \binom{n_i}{k} \phi_i^k (1-\phi_i)^{n_i-k},\\ n_i &= |(i \leftarrow)| + |(i \rightarrow)|\end{aligned} \quad (9)$$

Implementing Eq. 7 and 8 in *Stan* [28] allows us to automatically obtain both the expectation value and the local uncertainty of $\phi(x)$ (i.e., a set of position-dependent standard deviations, means, medians, 5- and 95-percentiles) following the rules of Bayesian statistics. Finally, the estimated $\phi(x)$ is applied to evaluate the force landscape and the corresponding potential energy landscape $U_{LTP}(x)$. Compilable code can be downloaded from *Github* (//github.com/tanyizhou/local-transition-probability).

V. POTENTIAL ENERGY LANDSCAPE RECONSTRUCTION

A. Reconstructing potential landscapes from experimental trajectories under equilibrium conditions

The three analysis methods discussed above are implemented to reconstruct potential energy landscapes at equilibrium using trajectory data extracted from experiments. $U_{PDF}(x)$ obtained from Eq. 1 is able to effectively depict features of the potential energy landscape where non-equilibrium forces are weak or absent, with results plotted in Fig. 3. First, we measured $U_{PDF}(x)$ for particles diffusing in a microfluidic channel with no external force applied. As expected, $U_{PDF}(x)$ is a nearly flat line in the channel as shown in Fig. 3(a). When line traps were generated and focused into the channel by HOTs, $U_{PDF}(x)$ clearly shows the position and the depth of the energy well. In Fig. 3(b), L1 indicates the energy landscape with one optical line trap. $U_{PDF}(x)$ here exhibits an energy well in the middle of the channel which matches the position of the line trap. In Fig. 3(c,d), L2 and L3 indicate the energy landscapes induced by two laser line traps with depth around 2 and 5 k_BT. The solved $U_{PDF}(x)$ shows the position and depth of the two energy landscapes.

For comparison, we applied the LTP method to reconstruct L0-L3 using the same trajectory ensembles. The energy landscapes reconstructed by the LTP approach [$U_{LTP}(x)$, solid lines in Fig. 3] are close to the ones reconstructed using the PDF approach. However, the LTP approach also allows us to estimate the error associated with the landscape estimation [grey areas in Fig. 3].

We further compare our LTP method with the SP method under equilibrium conditions. Energy landscapes $U_{SP}(x)$ estimated via the SP approach managed to show the features of a flat potential (L1), one energy minimum (L2) and two energy minimums (L3) [circles in Fig. 3(a-c)]. Note here, $\pi(x)$ is smoothed by a 100 nm boxcar filter to reduce noise as documented in [20]. By comparison, our LTP approach allows us to reconstruct landscapes with substantially reduced noise [solid lines in Fig. 3(a-c)]. Importantly, $U_{SP}(x)$ becomes invalid in the face of a deep energy barrier in Fig. 3(d). During the measurement, no particle starting near the left energy minimum exits from the right end of the channel, rendering $\pi(x) = constant$. However, $LTP(x)$ is able to pick up the moving direction of the particle and be used to calculate $U_{LTP}(x)$ [solid line in Fig. 3(d)].

B. Reconstructing potential landscapes from experimental trajectories out of equilibrium

Both the PDF and SP methods exhibit serious limitations when investigating systems out of equilibrium. We consider two forms of potential energy landscapes in non-equilibrium steady states. Firstly, no optical potential is coupled in the channel but a hydrodynamic flow exists between the two reservoirs. In the measurement reported for potential L4 [Fig. 4(a,c)], 193 particles are released at randomised starting positions along the channel, with 152 particles exiting to the left entrance of the channel and 41 particles leaving via the right entrance. In total, 80% of the particles exit through the left entrance of the channel, indicating a bias to the left direction. A constant bias, however, does not affect the time-averaged probability density and leads to a flat position histogram, so the PDF method resolved potential appears to be flat [$U_{PDF}(x)$, dashed line in Fig. 4(c)]. In the measurement for potential L5 [Fig. 4(b,d)], 206 particles exit via the left entrance and one particle exits via the right channel entrance. However, $U_{PDF}(x)$ reconstructed for L5 [dashed line Fig. 4(d)] still does not show the bias.

The splitting probability based $U_{SP}(x)$ is generally able to resolve $U(x)$ in non-equilibrium conditions, but requires a reliable estimation of the underlying splitting probability $\pi(x)$. $\pi(x)$ collected for L4 and L5 is plotted as squares in Fig. 4(a,b). In the case of a weak bias, $U_{SP}(x)$ describes the energy landscape reasonably but exhibits substantial fluctuations [circles in Fig. 4(c)]. In the data used for L5, $\pi(x)$ [squares in Fig. 4(b)] is essentially a constant $\pi(x < b) = 0$ with a data set consisting almost solely of left-exit events, which can not generate a valid $U_{SP}(x)$ via Eq. 2. In contrast, the potential energy landscape $U_{LTP}(x)$ (red line) reconstructed from $\phi(x)$ exhibits the bias in energy landscape L4 and L5. The strength of bias in the channel can be identified by comparing the value of $\phi(x)$ presented by circles

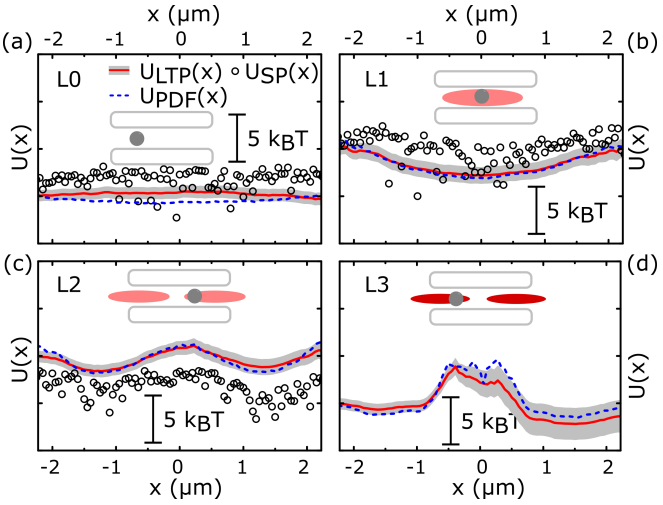

FIG. 3. Reconstruction of potential energy landscapes from experimental trajectories under equilibrium conditions. $U(x)$ is evaluated using the probability density approach $U_{PDF}(x)$ (dashed lines), the splitting probability method $U_{SP}(x)$ (circles) and the LTP approach $U_{LTP}(x)$ (solid lines) using the same trajectory ensembles. The shaded area represents the estimated standard deviation of $U_{LTP}(x)$. L1-L4 represent four different potential landscapes measured in channels.

in Fig. 4(a,b). Besides, slopes of $U_{LTP}(x)$ [solid lines in Fig. 4(c,d)] also shows the differences between the bias in two channels. To further validate our result, we calculate the average speed of particles across the channel then use Stokes' law to find the potential differences between two channel ends. We get ΔU equals 4.4 and 25.4 k_BT for L4 and L5, which matches the result from the LTP method.

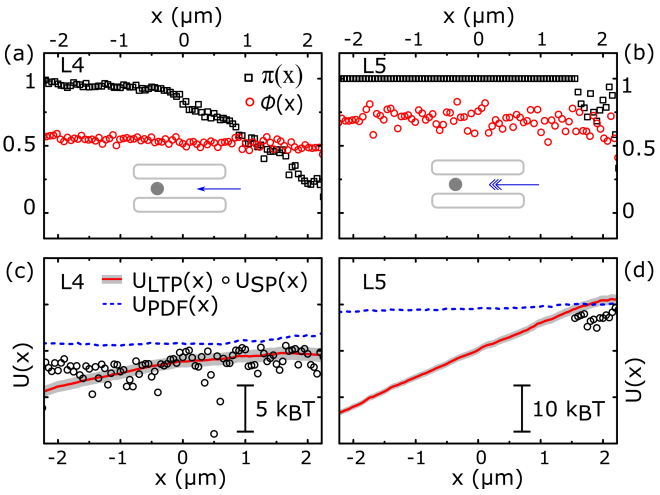

FIG. 4. Reconstructing potential energy landscapes from experimental trajectories in the presence of an external bias. (a,b) $\pi(x)$ is the splitting probability measured with two channel ends set as absorbing boundaries. $\phi(x)$ is the local transition probability measured in the same channel. (c,d) Energy landscape reconstructed by three methods using the same trajectory ensemble. Dashed lines show $U_{PDF}(x)$ obtained from the PDF method, circles show $U_{SP}(x)$ obtained from the SP method, solid lines show $U_{LTP}(x)$ obtained from our approach. The shaded area represents the estimated standard deviation of $U_{LTP}(x)$. Note that the relative value of $U(x)$ shows the difference of the potential energy landscape.

Secondly, we study potential energy landscapes with external bias forces and optical potentials coupled in the channel. Not surprisingly, the same limitations of the PDF and SP methods appear on the analysis of system with potential L6 and L7, as shown in Fig 5. $U_{PDF}(x)$ [dashed line in Fig. 5 (c,d)] only shows the contribution of optical traps to the potential energy landscape with bias information missing. Meanwhile, few transition events detected in the opposite direction of the bias make $\pi(x)$ constant in the region between -2.2 to -1 μm in Fig. 5(a), which cannot be used to calculate $U_{SP}(x)$ in L6. In the measurement for potential L7, no transition to the right end of the channel makes $\pi(x)$ a constant value over the whole observation region [Fig. 5(b)]. $U_{SP}(x)$ is therefore invalid and missing in Fig. 5(d). Crucially, our LTP approach allows us to recover the energy landscape successfully when a bias is superimposed on potential wells generated by laser line traps [solid lines in Fig. 5(c,d)].

In principle, larger ensemble sizes are all that is needed to obtain reliable results from the SP method. However,

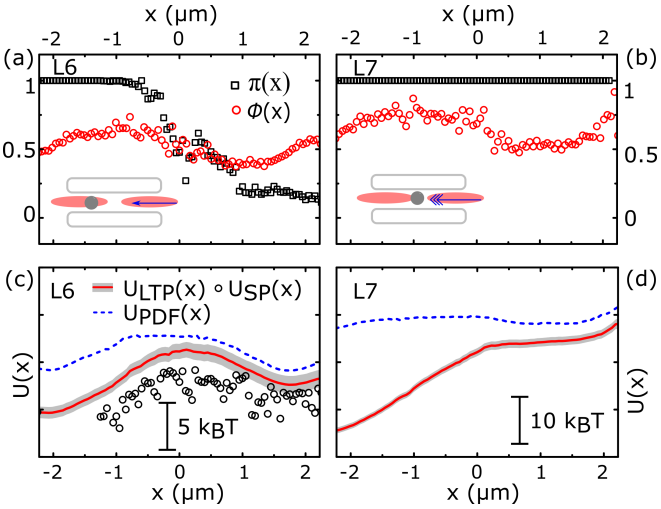

FIG. 5. Reconstructing potential energy landscapes from experimental trajectories in the presence of an optical potential and an external bias. (a,b) $\pi(x)$ measured with two channel ends set as absorbing boundaries.(c,d) Energy landscape reconstructed by three methods using the same trajectory ensemble, with dashed lines presenting $U_{PDF}(x)$, circles presenting $U_{SP}(x)$ and solid lines showing $U_{LTP}(x)$.

since the probability p of thermal activation across a potential with difference ΔU scales exponentially in ΔU, $p \propto \exp(\Delta U/k_BT)$, this solution may require exponentially more trajectories and become impossible to implement in practice. Compared to the SP method, the LTP approach appears to require significantly smaller trajectory ensembles to produce similarly reliable results. We compare the effect of ensemble sizes on the rebuilt potential energy landscape in Appendix B. Qualitatively, our method is subject to the same caveat: energetic barriers impede the motion of a particle, thus decrease the number of observed transition events and the reliability of the obtained result. Quantitatively, however, the energy differences that must be overcome to generate the local transitions analysed by our method are much smaller than the energy differences that must be overcome to generate the nonlocal exit events considered by the SP method.

VI. CONCLUSION

In summary, we developed a new approach to accurately characterise stationary one-dimensional potential landscape. Based on a local analysis of observed single-particle trajectories, our method correctly handles nonequilibrium scenarios as demonstrated in colloidal channel experiments. Our method improves on the conceptually similar splitting probability method by (i) allowing for the unbiased usage of small trajectory fragments (ii) providing us with systematic error estimates and (iii) increasing the accuracy of the obtained poten-

tial estimated at identical ensemble sizes. Experimentally, our approach demands no specialized equipment as it exclusively relies on the conventional microscopy technique, and is readily applied to single molecule measurements via fluorescence microscopy, force spectroscopy or electrophorosis.

ACKNOWLEDGMENTS

This work was supported by a Royal Society Research Grant (No.RG140203), a Wellcome Trust Strategic Seed Corn Fund, and a Start-up Grant from the University of Exeter awarded to S.P. U.F.K. was funded by an ERC Consolidator Grant (Designerpores No. 647144). Y.T. was supported by scholarship from Cavendish, Lundgren and Pannett Fund, Churchill College. A. T acknowledges... S.S acknowledges Graduate School BuildMoNa, the European Social Funds and the sächsische Forschergruppe DFG FOR 877 for financial support. J.G. acknowledges the support of the Winton Programme for the Physics of Sustainability and the European Union's Horizon 2020 research and innovation programme under ETN Grant No. 674979-NANOTRANS.

Appendix A: Deduction of mean displacement and mean square displacement of particles

To find the relationship between $\phi(x)$ and $U(x)$, we need to write down the average position displacement of the particle $x_{mean}(x)$ and the Mean Square Displacement (MSD) of a particle in a potential energy landscape. Assuming that the potential energy landscape is locally quadratic, the external force acting on the particle is

$$f_{ext} = F - (x - x0)\kappa + \xi \tag{A1}$$

where F denotes the force landscape, κ is the potential's local spring constant and ξ is random thermal noise. The f_{ext} in eq. A1 has to balance the drag force $\zeta\dot{x}(t)$, where ζ presents the friction coefficient. For $< x_{mean}(t) >$, the random part cancels out because $< \xi >= 0$, so we integrate

$$\zeta\dot{x}(t) = F - \kappa(x(t) - x0) \tag{A2}$$

which gives us

$$x_{mean}(\delta x, \Delta t) = e^{-\frac{\Delta t\kappa}{\zeta}}\left(\delta \mathrm{x} - \frac{F}{\kappa}\right) + \frac{F}{\kappa} \tag{A3}$$

For MSD ξ is important because the external force is deterministic, so the broadening of the particle density distribution comes from the random part, and unlike $< \xi >$, the squared expression $< \xi^2 >$ is not, in general zero. The fluctuation-dissipation theorem says that random thermal white noise satisfies $< \xi(t)\xi(t') >= 2\delta(t - t')k_BT\zeta$. Therefore, an extra force $A\delta(t)$ is added to Eq. A2 which generates a term $A\exp(-t\kappa/\zeta)/\zeta$ to the solution. The extra trajectory part caused by ξ is:

$$x_\xi(t) = \int_0^t \frac{\xi(T)\exp(\frac{-(t-T)\kappa}{\zeta})}{\zeta}\mathrm{d}T. \tag{A4}$$

Then we square Eq. A4:

$$< x_\xi(t)x'_\xi(t) >= < \int_0^t\int_0^t \xi(T)\xi(T')\exp(-(t-T)\kappa/\zeta) \exp(-(t-T')\kappa/\zeta)/\zeta^2\mathrm{d}T\mathrm{d}T' > \tag{A5}$$

Because exp and ζ are fully deterministic, we take the thermal average <> into the integral and get:

$$< x_\xi^2(t) >= \int_0^t\int_0^t \exp(-(t-T)\kappa/\zeta) \exp(-(t-T')\kappa/\zeta)/\zeta^2 < \xi(T)\xi(T') > \mathrm{d}T\mathrm{d}T' \tag{A6}$$

Now we replace $< \xi(T)\xi(T') >$ by $2\delta(T - T')k_BT\zeta$, which removes one of the integrals and the <> brackets:

$$< x_\xi^2(t) >= 2\int_0^t \frac{\exp(-2(t-T)\kappa/\zeta)}{\zeta}k_BT\mathrm{d}T \tag{A7}$$

After integration, we get

$$MSD(\Delta t) = \frac{k_BT\left(1 - e^{-\frac{2\Delta t\kappa}{\zeta}}\right)}{\kappa} \tag{A8}$$

Eq. A3 and A8 are put into a Gaussian propagator to write down the relationship between the probability density function of particles $p(x)$ and the force landscape $F(x)$.

Appendix B: Effect of the size of trajectories on the resolved potential energy landscape

In general, one would collect more experimental data to improve the estimation of $U(x)$. We consider this for our method by using different sizes of trajectory data from the same ensemble to rebuild a potential energy landscape at equilibrium. Using the LTP algorithm, the standard deviation of $U_{LTP}(x)$ decreases with the increased size of experimental trajectory data, as demonstrated by grey areas in Fig. 6(a-d). However, the LTP method managed to output reasonable potential using $N = 3966$ particle trajectories, with $U_{LTP}(x)$ plotted by a solid line in Fig. 6(a).

Importantly, $U_{LTP}(x)$ remains constant with different data sizes, as compared in Fig. 6(e). Meanwhile,

$U_{PDF}(x)$ is in a good agreement with $U_{LTP}(x)$ in all the tests. However, having a small size of trajectory ($N = 3966$) makes the SP incapable of reconstructing the potential energy landscape [circles in Fig. 6(a)]. The results of $U_{SP}(x)$ improve with increased numbers of trajectories used for the calculation, but $U_{SP}(x)$ is still significant more noisy compared to $U_{LTP}(x)$ in all the cases.

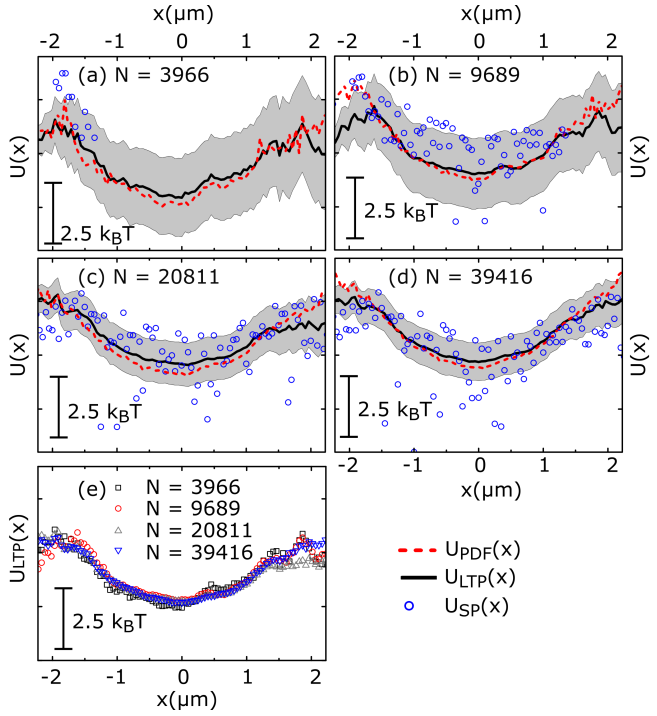

FIG. 6. Energy landscape reconstructed from ensembles of (a) N = 3966, (b) N = 9689, (c) N= 20811 and (d) N= 39416 experimental particle trajectories obtained by coupling a laser line in the centre of a microfluidic channel without any external bias. Comparison of the energy landscape estimated via the PDF ($U_{PDF}(x)$, dashed lines), the SP ($U_{SP}(x)$, circles) and the LTP approach ($U_{LTP}(x)$, solid lines and grey areas indicating mean and standard deviation, respectively). (e) shows the overlapping of $U_{LTP}(x)$ calculated by different N. Note that the relative value of $U(x)$ shows the difference of the potential energy landscape at different positions.

All three methods include binning the observation region x to measure the position density, the splitting probability and the local transition probability. The effect of the bin size is tested on an energy well at equilibrium with results plotted in Fig. 7. $U_{SP}(x)$ is affected by the bin size most severely. The fluctuation seen in $U_{SP}(x)$ becomes more significant with a smaller bin size by analysing the same trajectory ensemble (circles in Fig. 7). $U_{PDF}(x)$ also fluctuates more with a smaller bin size which provides less data for one bin [dashed lines in Fig. 7]. By comparison, the bin size on LTP analysis was found to have little effect on the rebuilt potential energy landscape and the error bar, as the solid lines and grey areas in Fig. 7(a-c) are almost identical.

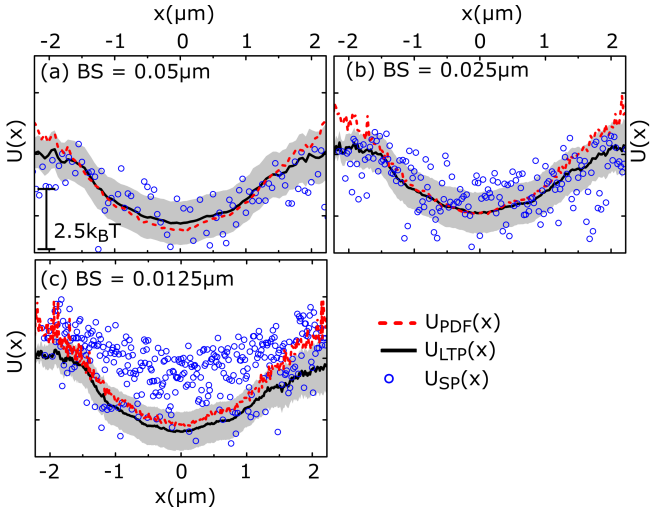

FIG. 7. Energy landscape reconstructed from the same ensemble of experimental particle trajectories obtained at equilibrium with a Bin Size (BS) of (a) $BS = 0.05$ μm, (b) $BS = 0.025$ μm and (c) $BS = 0.0125$ μm using the PDF ($U_{PDF}(x)$, dashed lines), the SP ($U_{SP}(x)$, circles) and the LTP approach ($U_{LTP}(x)$, solid lines and grey areas indicating mean and standard deviation, respectively). Note that the relative value of $U(x)$ shows the difference in the potential energy landscape.

[1] M. T. Woodside and S. M. Block, Annual review of biophysics **43**, 19 (2014).
[2] J. Camunas-Soler, M. Ribezzi-Crivellari, and F. Ritort, Annual Review of Biophysics **45**, 65 (2016).
[3] J. Han, S. W. Turner, and H. G. Craighead, **23** (1999).
[4] D. Kim, C. Bowman, J. T. Del Bonis-O'Donnell, A. Matzavinos, and D. Stein, Physical Review Letters **118**, 048002 (2017).
[5] S. E. Henrickson, M. Misakian, B. Robertson, and J. J. Kasianowicz, Physical Review Letters **85**, 3057 (2000).
[6] K. Misiunas, S. Pagliara, E. Lauga, J. R. Lister, and U. F. Keyser, Physical Review Letters **115**, 038301 (2015).
[7] E. Locatelli, M. Pierno, F. Baldovin, E. Orlandini, Y. Tan, and S. Pagliara, Physical Review Letters **117**, 038001 (2016).
[8] A. L. Thorneywork, R. E. Rozas, R. P. A. Dullens, and J. Horbach, 10.1103/PhysRevLett.115.268301.
[9] D. Babič, C. Schmitt, I. Poberaj, and C. Bechinger, Europhysics Letters **67**, 158 (2004).
[10] C. Schmitt, B. Dybiec, P. Hänggi, and C. Bechinger, Europhysics Letters **74**, 937 (2006).
[11] L. P. Faucheux, L. S. Bourdieu, P. D. Kaplan, and A. J. Libchaber, Physical Review Letters **74**, 1504 (1995).
[12] S.-H. Lee and D. G. Grier, Journal of physics. Condensed matter : an Institute of Physics journal **17**, S3685 (2005).
[13] M. P. MacDonald, G. C. Spalding, and K. Dholakia, Nature **426**, 421 (2003).
[14] L. L. McCann, L. L. McCann, M. Dykman, M. Dykman, B. Golding, and B. Golding, Nature **402**, 785 (1999).
[15] M. T. Woodside, P. C. Anthony, W. M. Behnke-Parks, K. Larizadeh, D. Herschlag, and S. M. Block, Science **314**, 1001 (2006).
[16] S. Pagliara, C. Schwall, and U. F. Keyser, Advanced materials **25**, 844 (2013).
[17] D. C. Rees, E. Johnson, and O. Lewinson, Nature Reviews Molecular Cell Biology **10**, 218 (2009).
[18] P. J. F. Henderson and S. a. Baldwin, Nature structural & molecular biology **20**, 654 (2013).
[19] J. D. Chodera and V. S. Pande, Physical Review Letters **107**, 1 (2011).
[20] A. P. Manuel, J. Lambert, and M. T. Woodside, Proceedings of the National Academy of Sciences , 201419490 (2015).
[21] S. Pagliara, C. Chimerel, R. Langford, D. G. a. L. Aarts, and U. F. Keyser, Lab on a chip **11**, 3365 (2011).
[22] S. Pagliara, S. L. Dettmer, K. Misiunas, L. Lea, Y. Tan, and U. F. Keyser, The European Physical Journal Special Topics **223**, 3145 (2014).
[23] J. E. Curtis, B. A. Koss, and D. G. Grier, Optics Communications **207**, 169 (2002).
[24] M. Padgett and R. Di Leonardo, Lab on a chip **11**, 1196 (2011).
[25] R. W. Bowman, G. M. Gibson, A. Linnenberger, D. B. Phillips, J. a. Grieve, D. M. Carberry, S. Serati, M. J. Miles, and M. J. Padgett, Computer Physics Communications **185**, 268 (2014).
[26] S. Pagliara, S. L. Dettmer, and U. F. Keyser, Physical Review Letters **113**, 048102 (2014).
[27] D. G. G. John C. Crocker, Journal of Colloid and Interface Science **310**, 298 (1996).
[28] B. Carpenter, A. Gelman, M. D. Hoffman, D. Lee, B. Goodrich, M. Betancourt, M. Brubaker, J. Guo, P. Li, and A. Riddell, Journal of Statistical Software **76** (2017), 10.18637/jss.v076.i01.